physica status solidi rrl
www.pss-rapid.com

Tailoring of Bound Exciton Photoluminescence Emission in WS_2 Monolayers

Reelika Kaupmees, Maarja Grossberg, Marcel Ney, Aswin Asaithambi, Axel Lorke, and Jüri Krustok*

Temperature- and laser power-dependent photoluminescence (PL) properties of the asymmetric defect-bound exciton band X_D in defective WS_2 monolayers, grown by chemical vapor deposition, are studied. Based on PL mapping, a monolayer region with an intensive X_D band emission at about 1.9 eV is chosen for further studies. The X_D band is thermally quenched above 180 K, and the thermal activation energy is found to be $E_a = 33 \pm 4$ meV. At $T = 15$ K, the X_D band intensity reveals a sublinear dependence with increasing excitation power and the peak position shows a blueshift of about 15 meV per decade of laser power. It is shown that the X_D band is related to the deep defect states within the band gap of WS_2.

Two-dimensional (2D) semiconductor atomic crystals, also known as transition metal dichalcogenides (TMDs), like MoS_2, $MoSe_2$, WS_2, and WSe_2, have attracted considerable attention because of their interesting physical properties and potential applications in various electronic and optoelectronic devices.[1–5] For example, monolayered TMDs have the advantage of being direct band gap semiconductors, unlike their 3D counterparts that have an indirect band gap.[6] Among these TMDs, WS_2 has the largest band gap in the visible spectral range, around 2.0 eV, and exhibits stronger photoluminescence (PL) emission than most other studied TMDs, making WS_2 atomic crystals excellent candidates for future optoelectronic devices.[7,8] The characteristic room temperature PL spectrum of a WS_2 monolayer consists of two excitonic peaks, *A* and *B*, resulting from the large valence band spin–orbit splitting of 425 meV.[9] The peak positions of *A* and *B* excitons in WS_2 are around 2.0 and 2.4 eV, respectively.[10] These values are found for mechanically exfoliated WS_2 monolayers, but the peak positions are really sensitive to the preparation method. In the case of WS_2 monolayers grown by chemical vapor deposition (CVD) onto Si/SiO_2 substrates, the *A* and *B* exciton peaks are usually detected at lower energies compared with the mechanically exfoliated layers or CVD-grown layers on other substrates.[11,12] This redshift is mostly caused by the strain in the as-grown monolayers on the Si/SiO_2 substrate.[13–15] In addition to the charge-neutral A^0 exciton peak, a charged trion A^- peak is also often found at about 43 meV lower energies.[16] At low temperatures ($T \approx 10$ K), a broad defect-bound exciton band (X_D) with a peak position of about 1.9 eV has been found to dominate the PL spectra.[17] This spectral region includes also a single-photon emission (a series of sharp peaks in the defect band region) that has been detected in the low-temperature PL spectra of WS_2 monolayers[18] and in other 2D compounds.[19–21] Excitons in the defect band region can be bounded to lattice defects.[22,23] In addition, Venanzi et al.[24] have shown that the defect-bound exciton band consists of excitons that are localized by physiosorbed gas molecules on the $MoSe_2$ monolayer surface. This phenomenon appears also in other TMDs like WS_2. Still, while *A* and *B* peaks have been studied extensively, the properties of the defect-bound exciton band are not fully understood. We have previously studied[25] the luminescence of excitons and trions in CVD-grown WS_2 monolayers and focus on the defect-bound exciton band properties using temperature and excitation power-dependent PL measurements.

WS_2 monolayers mainly grew in triangular islands with domain sizes up to several tens of micrometers; however, other shapes were observed as well. In **Figure 1**a, a scanning electron microscope (SEM) image of CVD-grown butterfly-like WS_2 monolayer is presented. The diameter of this monolayer is about 40 μm. Butterfly-like-shaped WS_2 monolayers have been seen in several studies.[26–28] These kinds of monolayers are reported to consist of two symmetrical wings with different atomic orientations, separated by a grain boundary.[27] Grain boundary usually includes multiple different misaligned atoms, creating extended defects to the material. The grain boundary area in the middle of the butterfly-shaped WS_2 monolayer is of particular interest, and therefore, it is a subject of this study. To confirm the high concentration of defects in the grain boundary, a room-temperature PL map from the monolayer was created. In Figure 1b, the PL peak position map of the A^0(neutral *A* exciton) peak is presented,

R. Kaupmees, Prof. M. Grossberg, Prof. J. Krustok
Department of Materials and Environmental Technology
Tallinn University of Technology
Ehitajate tee 5, Tallinn 19086, Estonia
E-mail: reelika.kaupmees@taltech.ee

M. Ney, A. Asaithambi, Prof. A. Lorke
Faculty of Physics and CENIDE
University of Duisburg-Essen
Lotharstr. 1, Duisburg 47057, Germany

Prof. J. Krustok
Division of Physics
Tallinn University of Technology
Ehitajate tee 5, Tallinn 19086, Estonia

The ORCID identification number(s) for the author(s) of this article can be found under https://doi.org/10.1002/pssr.201900355.

DOI: 10.1002/pssr.201900355

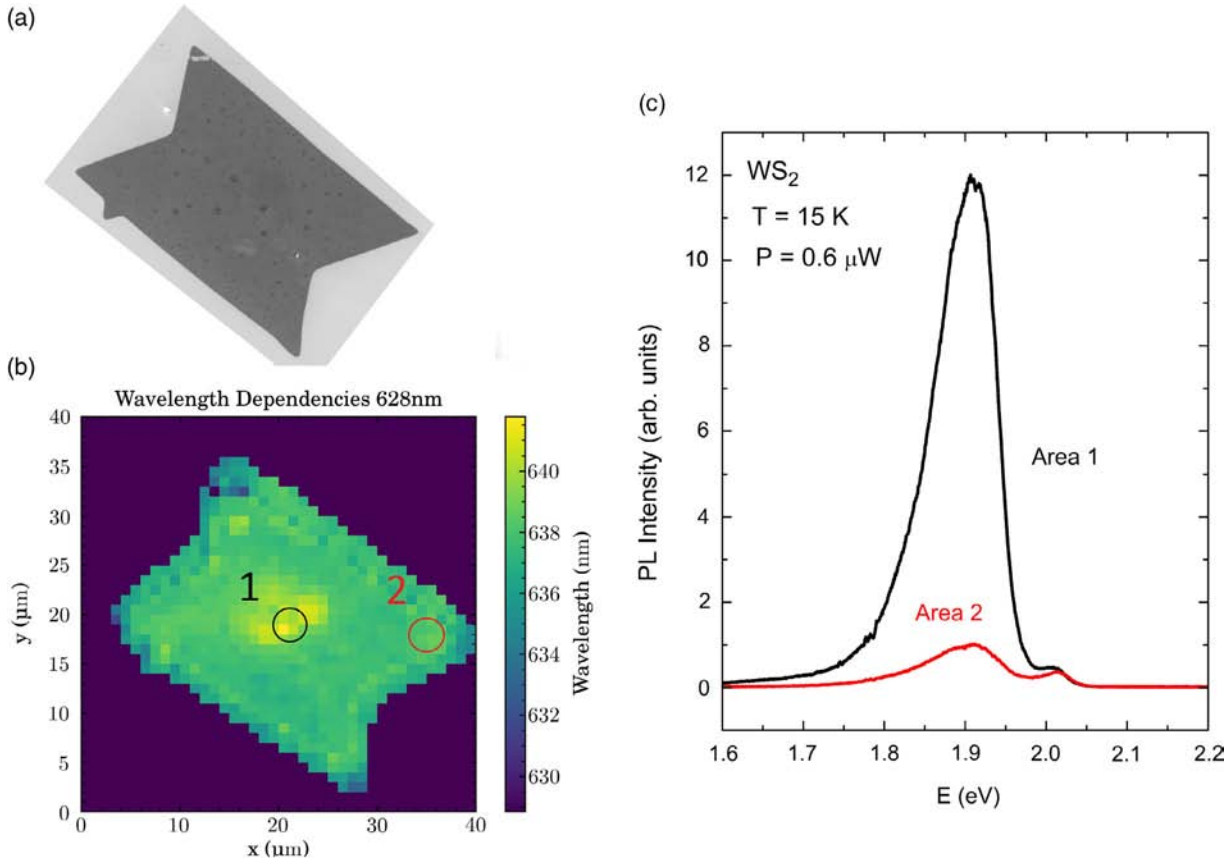

Figure 1. a) SEM picture of a butterfly-shaped WS_2 monolayer. b) 2D PL map showing the redshift of the A^0 exciton peak in the middle of the flake. c) Low-temperature ($T = 15$ K) PL spectra from different WS_2 monolayer areas marked as 1 and 2 in (b).

showing the redshift of the A^0 peak in the middle of the flake. It was shown that the high concentration of defects[29] and a possible tensile strain are the main reasons for this kind of peak shift of A^0 excitons in different TMD monolayers.[14,23,25] We chose this region with a high-intensity defect-bound exciton PL emission (see Figure 1c) for further studies and the results are presented below.

The room-temperature PL spectrum of this defective region shows only one asymmetrical A^0-exciton peak at $E_{max} = 1.940$ eV (**Figure 2**a). The peak is shifted to lower energy by about 80 meV when compared with mechanically exfoliated WS_2 monolayers.[16] In a previous study,[25] we observed an asymmetrical A^0 exciton peak at 1.951 eV in aged CVD-grown WS_2 and showed that, it was redshifted due to tensile strain. The intensity of the A^0 peak from our butterfly-shaped layer was around 100 times higher than the intensity of the A^0 peak from the double-layer WS_2, confirming that the WS_2 flake studied here is a monolayer.

The Raman spectrum from the CVD-grown WS_2 together with the fitting results is presented in **Figure 3**a. From the fitting, the positions of the main peaks, the in-plane mode $E^1_{2g}(\Gamma)$ at 355.0 cm^{-1} and the out-of-plane mode $A_{1g}(\Gamma)$ at 418.3 cm^{-1}, were determined. The separation between these peaks is $\Delta = 63.3\ cm^{-1}$. This value is somewhat higher than normally observed in WS_2 monolayers with better quality, where the

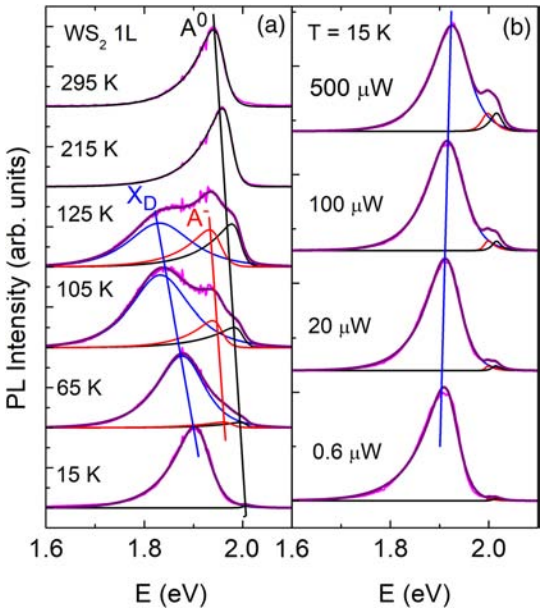

Figure 2. Normalized a) temperature and b) laser power dependencies ($T = 15$ K) of the PL spectrum of a WS_2 monolayer (purple lines). PL-fitting results with asymmetric hyperbolic secant functions are shown. Blue lines show the fitting results for the defect-bound exciton peak X_D, red lines for the trion peaks A^-, and black lines for the exciton peaks A^0.

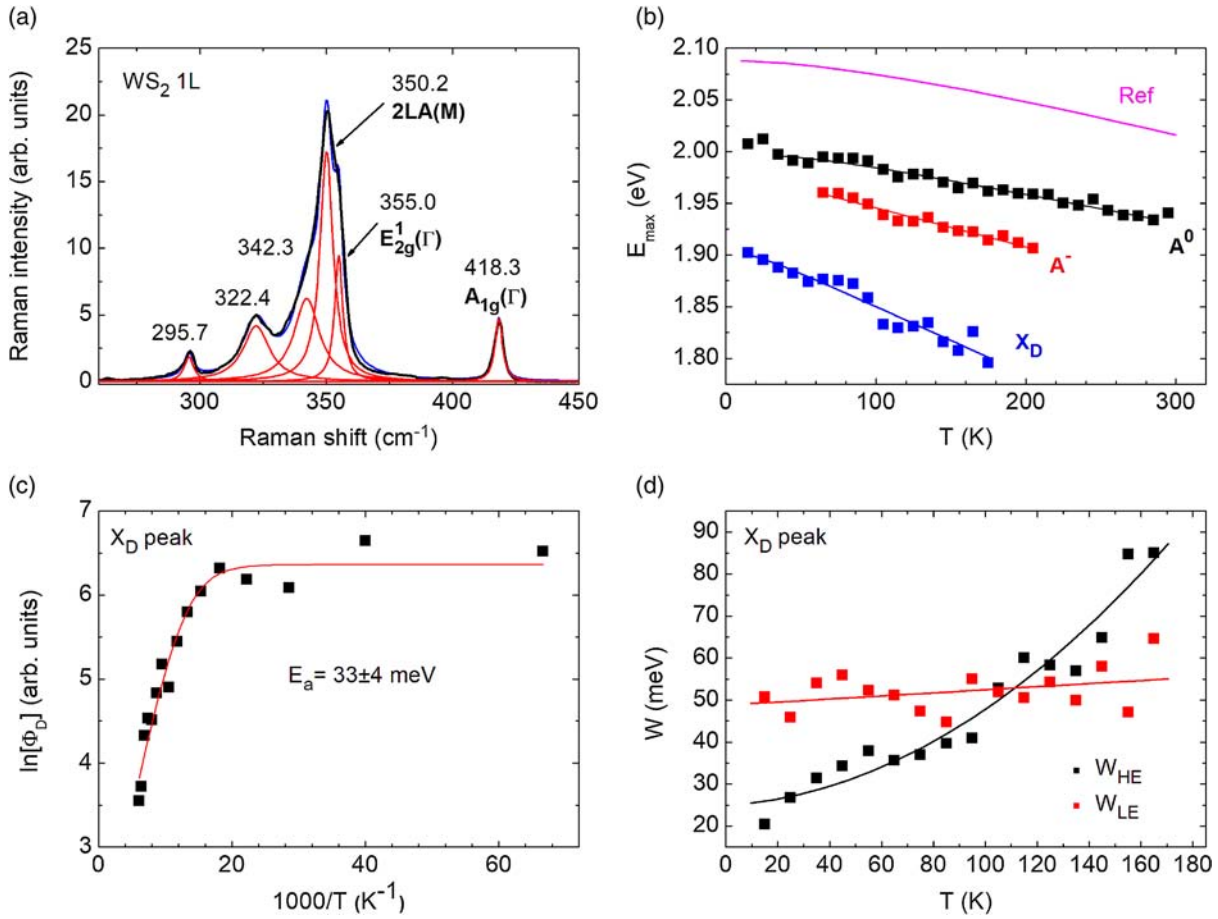

Figure 3. a) Raman spectrum from the WS_2 monolayer. Red lines show a result of spectral fitting with Lorentzian curves. The blue line presents the cumulative fitting result. b) Temperature dependence of the PL peak energies. Magenta line represents a temperature dependence of the A^0 peak taken from the study by Plechinger et al.[16] c) Arrhenius plot showing the activation energy of the X_D band. d) The width of high (W_{HE}) and low (W_{LE}) energy sides of the X_D band as a function of temperature. The lines are least squares fit to the data.

separation is usually in the range $\Delta = 61.5–62.4\,cm^{-1}$.[8,26,30,31] It is known that the tensile strain in WS_2 monolayers grown on the Si/SiO_2 substrate causes the in-plane Raman mode $E^1_{2g}(\Gamma)$ to redshift more than the $A_{1g}(\Gamma)$ peak,[32] which increases the separation between these peaks. The dominating mode in Figure 3a is $2LA(M)$ ($350.2\,cm^{-1}$) that has approximately three times the intensity of the $A_{1g}(\Gamma)$ mode, which is characteristic for the Raman spectra of WS_2 monolayers, measured with green laser excitation (514 nm,[30] 532 nm[33]). This fact and the peak separation value confirm once again that the studied butterfly-like flake is indeed a monolayer. Raman spectra show no dependence on the position on the flake, which indicates the same strain value throughout the flake.

All PL spectra were fitted using an asymmetric hyperbolic secant function: $I(E) = I_0/[\exp((E - E_M)/W_{HE}) + \exp(-(E - E_M)/W_{LE})]$, where W_{HE} and W_{LE} are related to the width of high- and low-energy sides of the PL band, respectively, while E_M is related to the peak position E_{max}.[25] In the case of the symmetrical peak, E_M is equal to E_{max}. The asymmetric hyperbolic secant function has been used previously to fit excitonic PL bands in WS_2[25] and $MoSe_2$[34] monolayers.

Low laser excitation power (5 μW) was chosen for the temperature-dependent PL measurements ($T = 15–295$ K) to have a more pronounced defect-bound exciton band X_D, compared with the exciton A^0 and trion A^- peaks. The temperature dependence of some characteristic PL spectra is presented in Figure 2a. An asymmetrical A^0 peak can be seen for the whole temperature range, although at low temperatures, it is relatively weak compared with the X_D band. The trion peak A^- appears at 65 K and disappears above 205 K (Figure 3b). The X_D emission band shows an asymmetric lineshape with a sharper high-energy cut-off and an exponential low-energy tail. This band is thermally quenched with increasing temperature and becomes invisible at temperatures above 180 K, as shown in Figure 3b. Moreover, the X_D band shows a redshift with increasing temperature and this shift is larger for the exciton and trion peaks, see Figure 3b. The redshift of the A^0 and A^- peaks with increasing temperature follows the same trend as the exciton peak in strain-free mechanically exfoliated WS_2 monolayers[16] shown as a reference in Figure 3b. A similar temperature dependence of the A^0 peak position was found also in the study by Gu et al.[33]

The fitting of the PL spectra measured at different temperatures revealed that the width related to the low energy side W_{LE} of the X_D band exhibits only a very weak increase with temperature (Figure 3d), whereas the width related to the high energy side W_{HE} shows a clear temperature dependence. All these features observed for the X_D band are usually considered as evidence of the disorder-related effects and are also typical for highly doped semiconductors like $CuInGaSe_2$[35] or $Cu_2ZnSnSe_4$.[36] As the random fluctuations of defect concentration or strain can cause band gap and electrostatic potential fluctuations, they may smear the band edges and form exponential tails of the density of states extending into the band gap. At low temperatures, excitons can be trapped by the localized states at the band tails, leading to the observed asymmetric lineshape of the PL spectra. In this case, the low-energy tail of the PL band reflects the energy distribution of the density of states within the band tails and has very weak temperature dependence.[35,37] At the same time, the high-energy side usually shows typical broadening with increasing temperature,[35] see Figure 3d. We therefore conclude that the X_D band is related to the deep defect states within the band gap and that the PL emission is caused by the excitons bound to these deep defects.

From the temperature dependence of integral intensity, the thermal activation energy $E_a = 33 \pm 4$ meV was determined for the defect-bound exciton X_D (Figure 3c) using the following equation[38]

$$\Phi(T) = \Phi_0/[1 + A_1 \exp(-E_a/kT)] \quad (1)$$

where Φ is the integral intensity of the PL band, A_1 is the process rate parameter, and E_a is thermal activation energy. A similar activation energy for the defect-bound exciton has been found not only in WS_2,[39] but also in other TMDs like WSe_2[22,40] and MoS_2.[41] When the temperature increases, bound excitons can be thermally activated into delocalized states and captured by the competing nonradiative recombination channels or recombine as free excitons. Therefore, it is expected that the intensity of the bound exciton emission decreases monotonically with increasing temperature. The carriers localized at shallow defect states are first thermally activated to the deeper states, leading to the redshift of X_D with increasing temperatures. Correspondingly, at low temperatures, the increasing excitation intensity is expected to cause band filling of the deeper localized energy states, giving rise to a blueshift of the X_D emission.

The laser excitation power dependence of the PL spectrum was measured at a low temperature ($T = 15$ K) in the range of $P = 0.6$–500 μW to study the nature of radiative recombination processes. In Figure 2b, the power series of the PL spectra are shown and it can be seen that the defect band X_D strongly dominates over the exciton and trion peaks especially at low laser powers. Furthermore, the X_D peak energy increases with increasing laser power (a straight blue line in Figure 2b), confirming the expected blueshift, caused by band-filling effects.

The integrated PL intensity Φ versus the laser excitation power P usually follows a power law dependence: $\Phi \approx P^k$.[42] The integrated PL intensity Φ as a function of excitation power P was investigated for all emission bands at $T = 15$ K, see **Figure 4**a. Both, exciton and trion peaks (A^0, A^-) show nearly linear dependence ($k \approx 0.9$), whereas the emission from the defect-bound exciton band X_D shows a different dependence and saturates at high excitation powers. It is also observed that the X_D band blueshifts as the excitation intensity increases and the rate of this shift is about 15 meV per decade of laser power (Figure 4b). This kind of blueshift is usually considered as the evidence of disorder-related effects in semiconductors.[23,35,43] We showed before that the random fluctuations of defect concentration or strain can cause band gap and potential fluctuations and form exponential tails in the density of localized states extending into the band gap. At low temperatures, the increasing excitation intensity will cause band filling of the localized energy states, giving rise to the blueshift of X_D emission.

It was shown theoretically that the PL intensity of the exciton-like transition should follow a power law $\Phi \approx P^k$ with $k \approx 1$. A value $k \ll 1$ indicates a recombination involving defect states.[42] However, the sublinear increase of the intensity of X_D band with laser power can be explained by the limited concentration of these deep defects leading to the saturation of the intensity of the X_D band at higher laser powers. A high concentration of deep defects usually leads to steeper increase of the PL intensity reflected by higher values of k, as reported by different

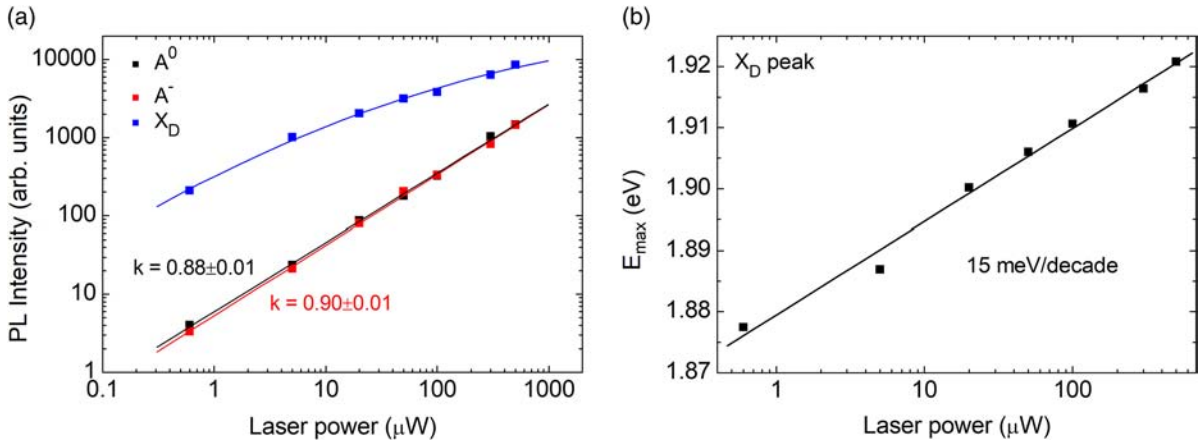

Figure 4. a) Integrated PL intensity Φ of different PL bands as a function of the laser power, plotted on a log–log scale. The lines are least squares fit to the data. b) X_D peak position dependence of the laser power. The line is least square fit to the data.

research groups, see for example the study by Shang et al.[44] Different k values for the defect band have been observed also in other materials like WSe_2[22,40] and MoS_2.[45] The sublinear dependence of the X_D band intensity in TMD monolayers was found also in WS_2[25] and MoS_2.[46]

The nature of these deep defects is not clear, but our experiments have shown that by using laser annealing, it is possible to reduce the intensity of the X_D band. The studied WS_2 monolayer was annealed with a focused laser beam with $P = 1500\,\mu W$ (power density $\approx 5 \times 10^8\,W/m^2$) for 5 min at a low temperature ($T = 15$ K). To study the effect of annealing, the PL spectra with a laser power of 0.6 μW before and after annealing were compared. Such a low excitation power was used, because the X_D band was found to be more pronounced when compared with A^0peak at low laser powers as shown in Figure 2b. Laser irradiation was found to reduce the relative intensity of the defect-bound exciton band about ten times compared with the A^0 exciton peak intensity, indicating that this type of annealing removes some physisorbed gas atoms from the WS_2 monolayer surface. This effect is rather interesting, suggesting that X_D band can be sensitive also to other forms of radiation, being useful for some applications. Similar effects have been observed also by other groups.[47,48]

The most probable intrinsic defect in the WS_2 monolayer could be a sulfur vacancy, V_S, with a reported depth of about 0.47–0.6 eV from the conduction band edge.[49–51] At the same time, grain boundaries and adsorbed atoms or molecules on the surface can also play an important role.

In conclusion, the defect-bound exciton band X_D at 1.9 eV was found to dominate the PL spectra of a WS_2 monolayer at low temperatures. It showed a larger redshift than the A^- and A^0 peaks with increasing temperature. The width of the low-energy side W_{LE} of the X_D band that reflects the energy distribution of the density of the states within the band tails showed a very weak temperature dependence, whereas the high-energy side (W_{HE}) demonstrated typical broadening. A thermal activation energy of $E_a = 33 \pm 4$ meV was found for the X_D band. The intensity of the X_D band showed a sublinear dependence with laser power, and a blueshift of about 15 meV per decade of laser power was detected for the PL band position. It is proposed that the X_D band is related to the deep defect-bound excitons and the most probable deep defect could be V_S, whereas the structural defects and adsorbed atoms could also be the cause of these deep defects.

Experimental Section

WS_2 monolayers were grown by CVD on a Si substrate with a 275 nm-thick SiO_2 layer using WO_3 and S precursors. In a two-zone furnace, the temperature in the S zone was 200 °C and in the WO_3 zone 850 °C. A mix of N_2 and H_2 (9%) was used as the carrier gas with a flow rate of 132 sccm. The Si/SiO_2 substrate was placed face down next to the WO_3 precursor.

Raman measurements were carried out in backscattering configuration using a Horiba LabRAM HR800 Micro-Raman system with a spectral resolution better than 1 cm^{-1}, equipped with a cooled multichannel charge-coupled device (CCD) detection system. A Nd-YAG laser (wavelength: 532 nm) was used for excitation. A 0.50 m focal length monochromator ACTON 2500i and an Oxxius - LMX-532 laser (wavelength of 532 nm) with different powers were used for micro-PL measurements. For PL detection, a liquid nitrogen-cooled CCD camera was used. A continuous-flow liquid helium cryostat Janis ST-500 was used for the temperature-dependent ($T = 15$–295 K) PL measurements. The laser spot size was about 2 μm in diameter for both setups.

The high-resolution SEM HR-SEM Zeiss Merlin was used to study the morphology of monolayers.

Acknowledgements

This work was supported by institutional research funding IUT (IUT19-28) of the Estonian Ministry of Education and Research and by the European Union through the European Regional Development Fund, Project TK141. A.A. would like to thank the Max Planck Society for providing a doctoral fellowship through IMPRS-SurMat.

Conflict of Interest

The authors declare no conflict of interest.

Keywords

chemical vapor deposition, defects, monolayers, photoluminescence, WS_2

Received: June 19, 2019
Revised: July 17, 2019
Published online:

[1] K. S. Novoselov, D. Jiang, F. Schedin, T. J. Booth, V. V. Khotkevich, S. V. Morozov, A. K. Geim, *Proc. Natl. Acad. Sci. USA* **2005**, *102*, 10451.
[2] H. Tan, Y. Fan, Y. Zhou, Q. Chen, W. Xu, J. H. Warner, *ACS Nano* **2016**, *10*, 7866.
[3] O. Lopez-Sanchez, D. Lembke, M. Kayci, A. Radenovic, A. Kis, *Nat. Nanotechnol.* **2013**, *8*, 497.
[4] B. Radisavljevic, A. Radenovic, J. Brivio, V. Giacometti, A. Kis, *Nat. Nanotechnol.* **2011**, *6*, 147.
[5] S. B. Desai, S. R. Madhvapathy, A. B. Sachid, J. P. Llinas, Q. Wang, G. H. Ahn, G. Pitner, M. J. Kim, J. Bokor, C. Hu, H.-S. P. Wong, A. Javey, *Science* **2016**, *354*, 99.
[6] H. Terrones, F. Lopez-Urias, M. Terrones, *Sci. Rep.* **2013**, *3*, 1549.
[7] J. Gusakova, X. Wang, L. L. Shiau, A. Krivosheeva, V. Shaposhnikov, V. Borisenko, V. Gusakov, B. K. Tay, *Phys. Status Solidi A* **2017**, *214*, 1700218.
[8] H. R. Gutiérrez, N. Perea-López, A. L. Elías, A. Berkdemir, B. Wang, R. Lv, F. López-Urías, V. H. Crespi, H. Terrones, M. Terrones, *Nano Lett.* **2013**, *13*, 3447.
[9] D. W. Latzke, W. Zhang, A. Suslu, T. R. Chang, H. Lin, H. T. Jeng, S. Tongay, J. Wu, A. Bansil, A. Lanzara, *Phys. Rev. B* **2015**, *91*, 235202.
[10] A. T. Hanbicki, M. Currie, G. Kioseoglou, A. L. Friedman, B. T. Jonker, *Solid State Commun.* **2015**, *203*, 16.
[11] L. Su, Y. Yu, L. Cao, Y. Zhang, *Nano Res.* **2015**, *8*, 2686.
[12] Y. Yu, Y. Yu, C. Xu, Y. Q. Cai, L. Su, Y. Zhang, Y. W. Zhang, K. Gundogdu, L. Cao, *Adv. Funct. Mater.* **2016**, *26*, 4733.
[13] Y. Wang, C. Cong, W. Yang, J. Shang, N. Peimyoo, Y. Chen, J. Kang, J. Wang, W. Huang, T. Yu, *Nano Res.* **2015**, *8*, 2562.
[14] J. Krustok, T. Raadik, R. Jaaniso, V. Kiisk, I. Sildos, M. Marandi, H.-P. Komsa, B. Li, X. Zhang, Y. Gong, P. M. Ajayan, *Appl. Phys. Lett.* **2016**, *109*, 253106.
[15] R. Kaupmees, H. Komsa, J. Krustok, *Phys. Status Solidi B* **2019**, *256*, 1800384.
[16] G. Plechinger, P. Nagler, J. Kraus, N. Paradiso, C. Strunk, C. Schüller, T. Korn, *Phys. Status Solidi RRL – Rapid Res. Lett.* **2015**, *9*, 457.

[17] V. Orsi Gordo, M. A. G. Balanta, Y. Galvão Gobato, F. S. Covre, H. V. A. Galeti, F. Iikawa, O. D. D. Couto Jr, F. Qu, M. Henini, D. W. Hewak, C. C. Huang, *Nanoscale* **2018**, *10*, 4807.
[18] C. Palacios-Berraquero, D. M. Kara, A. R.-P. Montblanch, M. Barbone, P. Latawiec, D. Yoon, A. K. Ott, M. Loncar, A. C. Ferrari, M. Atatüre, *Nat. Commun.* **2017**, *8*, 15093.
[19] A. Srivastava, M. Sidler, A. V. Allain, D. S. Lembke, A. Kis, A. Imamoglu, *Nat. Nanotechnol.* **2015**, *10*, 491.
[20] Y. M. He, G. Clark, J. R. Schaibley, Y. He, M. C. Chen, Y. J. Wei, X. Ding, Q. Zhang, W. Yao, X. Xu, C. Y. Lu, J. W. Pan, *Nat. Nanotechnol.* **2015**, *10*, 497.
[21] P. Tonndorf, R. Schmidt, R. Schneider, J. Kern, M. Buscema, G. A. Steele, A. Castellanos-Gomez, H. S. J. van der Zant, S. Michaelis de Vasconcellos, R. Bratschitsch, *Optica* **2015**, *2*, 347.
[22] Z. Wu, W. Zhao, J. Jiang, T. Zheng, Y. You, J. Lu, Z. Ni, *J. Phys. Chem. C* **2017**, *121*, 12294.
[23] Z. Wu, Z. Ni, *Nanophotonics* **2017**, *6*, 1219.
[24] T. Venanzi, H. Arora, A. Erbe, A. Pashkin, S. Winnerl, M. Helm, H. Schneider, *Appl. Phys. Lett.* **2019**, *114*, 172106.
[25] J. Krustok, R. Kaupmees, R. Jaaniso, V. Kiisk, I. Sildos, B. Li, Y. Gong, *AIP Adv.* **2017**, *7*, 65005.
[26] Y. Zhang, Y. Zhang, Q. Ji, J. Ju, H. Yuan, J. Shi, T. Gao, D. Ma, M. Liu, Y. Chen, X. Song, H. Y. Hwang, Y. Cui, Z. Liu, *ACS Nano* **2013**, *7*, 8963.
[27] Y.-C. Lin, C.-H. Yeh, H.-C. Lin, M.-D. Siao, Z. Liu, H. Nakajima, T. Okazaki, M.-Y. Chou, K. Suenaga, P.-W. Chiu, *ACS Nano* **2018**, *12*, 12080.
[28] L. Dong, Y. Wang, J. Sun, C. Pan, Q. Zhang, L. Gu, B. Wan, C. Song, F. Pan, C. Wang, Z. Tang, J. Zhang, *2D Mater.* **2019**, *6*, 15007.
[29] P. K. Chow, R. B. Jacobs-Gedrim, J. Gao, T. M. Lu, B. Yu, H. Terrones, N. Koratkar, *ACS Nano* **2015**, *9*, 1520.
[30] A. Berkdemir, H. R. Gutiérrez, A. R. Botello-Méndez, N. Perea-López, A. L. Elías, C. I. Chia, B. Wang, V. H. Crespi, F. López-Urías, J. C. Charlier, H. Terrones, M. Terrones, *Sci. Rep.* **2013**, *3*, 1.
[31] K. M. McCreary, A. T. Hanbicki, G. G. Jernigan, J. C. Culbertson, B. T. Jonker, *Sci. Rep.* **2016**, *6*, 19159.
[32] A. M. Dadgar, D. Scullion, K. Kang, D. Esposito, E. H. Yang, I. P. Herman, M. A. Pimenta, E. G. Santos, A. N. Pasupathy, *Chem. Mater.* **2018**, *30*, 5148.
[33] H. Gu, L. Chen, Y. Lu, F. Tian, Z. Zhang, K. Xu, J. Wu, V. D. Botcha, K. Li, X. Liu, *Jpn. J. Appl. Phys.* **2018**, *57*, 60309.
[34] J. S. Ross, S. Wu, H. Yu, N. J. Ghimire, A. M. Jones, G. Aivazian, J. Yan, D. G. Mandrus, D. Xiao, W. Yao, X. Xu, *Nat. Commun.* **2013**, *4*, 1474.
[35] J. Krustok, H. Collan, M. Yakushev, K. Hjelt, *Phys. Scr.* **1999**, *T79*, 179.
[36] M. V. Yakushev, M. A. Sulimov, J. Márquez-Prieto, I. Forbes, J. Krustok, P. R. Edwards, V. D. Zhivulko, O. M. Borodavchenko, A. V. Mudryi, R. W. Martin, *Sol. Energy Mater. Sol. Cells* **2017**, *168*, 69.
[37] J. Krustok, J. Raudoja, M. Yakushev, R. D. Pilkington, H. Collan, *Phys. Status Solidi A* **1999**, *173*, 483.
[38] J. Krustok, H. Collan, K. Hjelt, *J. Appl. Phys.* **1997**, *81*, 1442.
[39] V. Carozo, Y. Wang, K. Fujisawa, B. R. Carvalho, A. Mccreary, S. Feng, Z. Lin, C. Zhou, N. Perea-lópez, A. L. Elías, B. Kabius, V. H. Crespi, M. Terrones, *Sci. Adv.* **2017**, *3*, 1602813.
[40] Z. Wu, Z. Luo, Y. Shen, W. Zhao, W. Wang, H. Nan, X. Guo, L. Sun, X. Wang, Y. You, Z. Ni, *Nano Res.* **2016**, *9*, 3622.
[41] N. Saigal, S. Ghosh, *Appl. Phys. Lett.* **2016**, *109*, 122105.
[42] T. Schmidt, K. Lischka, W. Zulehner, *Phys. Rev. B.* **1992**, *45*, 8989.
[43] A. Jagomägi, J. Krustok, M. Grossberg, M. Danilson, J. Raudoja, *Phys. Status Solidi A* **2006**, *203*, 949.
[44] J. Shang, X. Shen, C. Cong, N. Peimyoo, B. Cao, M. Eginligil, T. Yu, *ACS Nano* **2015**, *9*, 647.
[45] J. Shang, C. Cong, X. Shen, W. Yang, C. Zou, N. Peimyoo, B. Cao, M. Eginligil, W. Lin, W. Huang, T. Yu, *Phys. Rev. Mater.* **2017**, *1*, 74001.
[46] S. Tongay, J. Suh, C. Ataca, W. Fan, A. Luce, J. S. Kang, J. Liu, C. Ko, R. Raghunathanan, J. Zhou, F. Ogletree, J. Li, J. C. Grossman, J. Wu, *Sci. Rep.* **2013**, *3*, 2657.
[47] Z. He, X. Wang, W. Xu, Y. Zhou, Y. Sheng, Y. Rong, J. M. Smith, J. H. Warner, *ACS Nano* **2016**, *10*, 5847.
[48] V. Orsi Gordo, M. A. G. Balanta, Y. Galvão Gobato, F. S. Covre, H. V. A. Galeti, F. Iikawa, O. D. D. Couto Jr, F. Qu, M. Henini, D. W. Hewak, C. C. Huang, *Nanoscale* **2018**, *10*, 4807.
[49] J. Wei, Z. Ma, H. Zeng, Z. Wang, Q. Wei, P. Peng, *AIP Adv.* **2012**, *2*, 42141.
[50] H. Liu, N. Han, J. Zhao, *RSC Adv.* **2015**, *5*, 17572.
[51] X. Zhao, X. Dai, C. Xia, T. Wang, *Superlattices Microstruct.* **2015**, *85*, 339.